

James M. Kirkness-Duncombe¹, Nicholas J. Lawson¹, Gareth A. Vio², Scott D. Moss² & David J. Munk²

¹The University of Sydney, Department of Aeronautical Engineering ²Defence Science and Technology Group, Aerospace Division

Abstract

This paper explores the use of high-energy cavity environments as a power source for structural health monitoring systems. It focuses on harnessing the aeroacoustic energy in a rectangular cavity setting, through the development and deployment of a relaxor-ferroelectric single-crystal energy harvester device. A series of wind tunnel tests were conducted to explore the energy harvesting capabilities of the device, when located on the experimental cavity floor panel, for varying cavity geometries. The harvester consists of 0.175 mm thick [011] poled $Mn-Pb(Mg_{1/3}Nb_{2/3})O_3-Pb(Zr,Ti)O_3$ (or Mn-PMN-PZT) single crystal fiber composite (SFC), bonded to spring steel flat plate. The device was tested with the SFC orientated in a parallel and perpendicular (with respect to the free stream airflow) configuration for all cavity geometries, at a free stream velocity of 60 m/s. The results indicate that under optimum tunnel conditions the SFC in the perpendicular orientation produced the maximum average power for all geometries tested.

Keywords: Aeroacoustics, Energy Harvesting, Cavity Flow, Piezoelectric

1. Introduction

Regular evaluation of an aircraft's structural health is essential to ensure its longevity and safe operation throughout its service life. These assessments often involve frequent, resource-intensive maintenance checks, aimed at identifying and mitigating the effects of structural fatigue, before they develop into critical failures. Structural fatigue in aircraft tends to occur due to repetitive and fluctuating loads experienced during normal flight operations, including changes in pressure, temperature, and various aerodynamic loads. Over time, these cyclical stresses can initiate small cracks in the aircraft's structure, which can grow and combine, leading to significant structural damage if not detected and repaired promptly [1, 2].

The need for frequent checks is driven by the fact that structural fatigue damage often progresses in an unpredictable manner. Early-stage cracks may not be detectable using standard inspection methods, and by the time they are visible, may already have compromised the structural integrity of the aircraft. Consequently, regular resource-intensive maintenance checks must be performed to detect any signs of fatigue as early as possible. Traditional inspection methods such as visual inspections and non-destructive testing (NDT) techniques, including ultrasonic testing, eddy current testing, and radiography, are labour intensive and time-consuming. They also require the aircraft to be taken out of service, affecting the availability and operational efficiency of the fleet, contributing to an increase in operational costs. Furthermore, these methods may not always provide a comprehensive assessment of the structural health of the aircraft, particularly in areas that are difficult to access or thoroughly inspect [3, 4].

Structural Health Monitoring (SHM) technologies have emerged as a transformative solution that provides continuous real-time monitoring of aircraft structural conditions, particularly in areas known to

be susceptible to high levels of fatigue. These advanced systems represent a significant step forward from traditional maintenance practices, which are often reactive and scheduled based on fixed intervals rather than on the real-time condition of the aircraft. SHM technologies enable a proactive approach by continuously collecting data on the structural health of the aircraft, allowing timely interventions before minor issues escalate to critical failures [5, 6, 7]. The effectiveness of SHM systems is particularly evident in high-stress areas such as wing joints, fuselage, tail sections, and cavity regions where repeated stress cycles can cause fatigue cracks and other structural damage. Focussing on these areas. SHM systems help maintain the structural integrity of the aircraft and improve overall flight safety through the use of a network of sensors embedded within the aircraft structure to detect and measure parameters such as strain, temperature, and vibration, providing a continuous stream of data that can be analysed to assess the structural health of the aircraft in real time [8, 9, 6]. These sensors send data to a central processing unit, where sophisticated algorithms analyse the information to detect anomalies and predict potential failures. This can help extend the useful life of aircraft components and enhance the safety and reliability of flight operations. This shift from reaction-based scheduled maintenance to condition-based maintenance is a significant advancement, aligning maintenance efforts more closely with the actual needs of the aircraft, resulting in optimised resource use and minimising downtime and thus operational cost [9].

Despite the advantages that SHM systems can provide, a primary challenge persists: an efficient and reliable power supply for these sensors, especially when placed in areas that are particularly difficult to access or are completely inaccessible. These areas often require non-intrusive methods for power delivery. Although common solutions to power SHM technologies are readily available, they often present limitations that can have a negative impact on an aircraft's overall efficiency. Connecting SHM technologies to the aircraft's main power supply with direct wire connections can lead to a significant increase in weight, reducing efficiency and thus affecting the operational cost of the aircraft. The use of batteries to power SHM technologies, while providing a wireless solution, introduces risks such as overheating and thermal runaway. Thermal runaway is a critical issue with lithium-ion batteries, where excessive heat triggers a chain reaction leading to fires or explosions [10]. These incidents are particularly concerning in aviation, where battery failures can have catastrophic consequences. Furthermore, regulatory limitations imposed by aviation governing bodies add to the challenges, where strict guidelines govern the use, transport, and disposal of lithium-ion batteries to mitigate risks. These regulations include safety checks and restrictions on the quantity and type of batteries that can be used, which can complicate the integration of SHM systems [10].

The dynamic environment in which aircraft operate, characterised by varied aerodynamic, maneuvering, thermal, and vibrational loads, not only inherently subjects the structure to complex and repetitive stresses, but also presents a unique opportunity to harness these forces for beneficial purposes. An area that experiences high levels of fatigue during normal operating conditions are cavity environments, such as wheel wells, weapons bays, optical bays, and cargo bays. The interaction of airflow within a cavity structure (as shown in Figure 1) causes vortex shedding and pressure oscillations at the leading edge of the cavity. These vortices travel downstream and interact with the cavity aft wall, creating high-intensity pressure waves that propagate back upstream and generate a feedback loop [3, 4]. These complex interactions lead to aeroacoustic resonances known as Rossiter modes, which can coincide with the natural frequencies of the structure, leading to increased vibrational stress and material fatigue [2, 11]. The complexity of predicting and mitigating these aeroacoustic effects, coupled with the inaccessibility of these cavities in some cases, poses significant challenges when considering the structural integrity and maintenance of aircraft.

Converting this self-sustaining aeroacoustic energy into electrical energy using piezoelectric energy harvesting devices during high-fatigue instances, such as when wheel wells and weapon bays are open during flight operations, presents a unique solution for powering SHM systems. Piezoelectric devices have been shown to generate sufficient power without the need for a continuous energy supply, demonstrating their practicality in intermittent high-energy scenarios [12, 13] and thus their

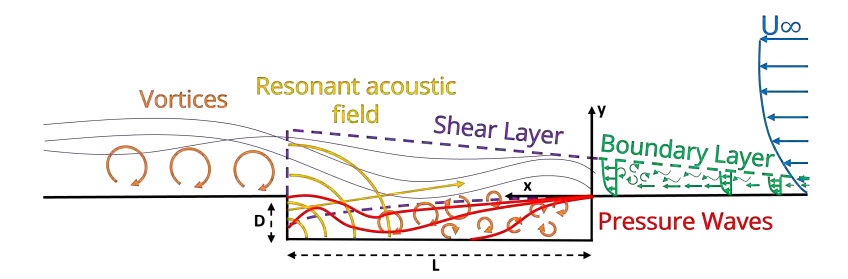


Figure 1 – Cavity flow features.

potential to be a viable solution for powering SHM systems in active cavity regions of operational aircraft. Using this energy to power SHM systems allows them to gain more autonomy and reduce dependence on traditional power sources, mitigating issues related to weight, safety, regulations, and operational efficiency. Ensuring that enough energy can be harvested by a piezoelectric harvesting device, particularly during high-fatigue instances, requires extensive testing and optimisation of the energy harvesting device, in conjunction with developing a robust understanding of the flow characteristics of a cavity environment.

A computational study conducted by Matthew Schipper [6] has provided critical insights into optimising the geometry and orientation of single crystal fiber composite (SFC) piezoelectric energy harvesting devices for maximum energy generation. This study used detailed multiphysics modelling to compare the performance of piezoelectric devices mounted in parallel and perpendicular orientations with respect to free stream airflow (U∞) within a structural cavity. The models predicted that the perpendicular orientation significantly increased the in-plane strain experienced by the piezoelectric material, leading to a higher energy output [6]. The key findings of this study showed that the perpendicular orientation of the piezoelectric device resulted in a more uniform and larger strain distribution along the device, as seen in Figures 2 and 3, enhancing the piezoelectric effect and thus energy generation. The computational model showed that the perpendicular device should be capable of generating approximately 3-4 times more power than the parallel device under similar conditions, confirmed by initial baseline experimental results of the parallel and perpendicular devices. The adoption of a perpendicular orientation aims to maximise the energy harvested from aeroacoustic energy in aircraft cavities and enhance the efficiency and effectiveness of SHM systems in aerospace applications.

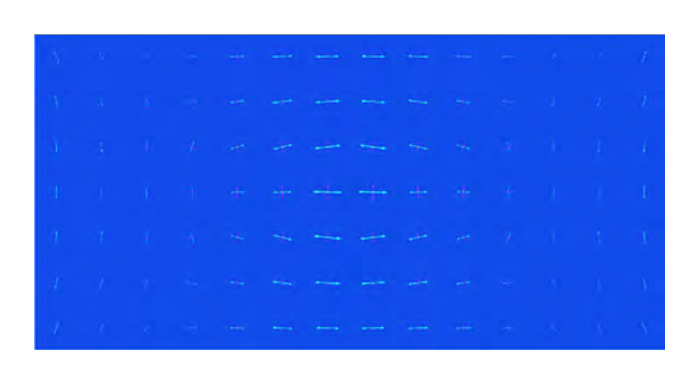
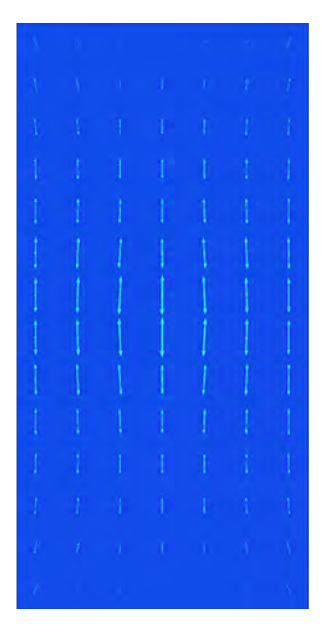


Figure 2 – Modeled principle strain distribution of Figure 3 – Modeled principle strain distribution of SFC in parallel configuration [6].



SFC in perpendicular configuration [6].

The findings of these computational studies were instrumental in guiding the design and orientation of the piezoelectric devices used in further experiments. By adopting the perpendicular orientation, the aim was to maximise the energy harvested from aeroacoustic energy within cavity regions, thus enhancing the efficiency and effectiveness of SHM systems in aerospace applications. In this paper, experimental wind tunnel results for the two parallel and perpendicular energy harvesting devices located centrally on a rectangular cavity floor panel are presented.

2. Experiment Test Setup and Method

All experiments were carried out at The University of Sydney using the Department of Aeronautical Engineering $4\,\mathrm{ft}\times3\,\mathrm{ft}$ closed-circuit low-speed wind tunnel. The wind tunnel consists of two $4\,\mathrm{ft}\times3\,\mathrm{ft}$ test sections, where the aft test section shown in Figures 4 and 5, was used to carry out all experiments.

A wind tunnel wooden floor test section was modified to incorporate a $456 \text{ mm} \times 210 \text{ mm}$ rectangular cutout (highlighted in Figure 6) which would serve as the opening of the cavity. A rectangular cavity was developed using 8 mm thick clear perspex. Each face was cut precisely and bonded together using self-tapping screws and adhesive, ensuring that all joints were sealed to mitigate internal pressure loss during experimental testing.



Figure 4 – The University of Sydney 4 ft \times 3 ft wind tunnel test section - side profile.



Figure 5 – The University of Sydney 4 ft \times 3 ft wind tunnel test section - front profile.

2.1 Cavity Model

The cavity model consists of two main components: the main cavity outer box and a smaller cavity inner box (length slide), highlighted in Figures 6 and 7. This design allows the cavity inner box to rest and slide along the floor of the cavity outer box in the lengthwise direction, enabling the adjustment of the cavity length to a desired geometry for testing. For a desired length, wooden block inserts (highlighted in Figure 6) are mounted to the $456~\rm mm~\times~210~mm$ rectangular cutout of the wooden wind tunnel floor panel. These inserts sit on top of the cavity inner box, ensuring the internal cavity surface remains uninterrupted and the external surface, or wind tunnel floor, maintains an even profile outside of the desired cavity opening. The forward face sections of the cavity inner and outer boxes had 8 mm thick horizontal slits cut to various depths. This design allows the insertion of a 8 mm thick perspex panel through each corresponding slit, serving as the cavity floor panel (depth slide). Additionally, the cavity floor panel was designed to house the energy harvesting device, ensuring that after bonding the device to the floor panel, it sits flush with the surface of the cavity floor. The

adjustable depth slide allows for the cavity depth to be changed to achieve a specific geometry for testing. Where the depth slide sits below one of these slit, perspex inserts are placed in each slit to ensure there is no pressure loss inside the cavity.

The main cavity outer box has two aluminum L-brackets mounted to the outer topmost sections of both side walls of the cavity, allowing the cavity to be mounted and aligned with the $456~\text{mm}\times210~\text{mm}$ rectangular cutout section on the bottom of the wind tunnel wooden test section, as shown in Figures 6 and 7. These design considerations enable the cavity geometry to be modified for 9 lengths and 9 depths, producing 81 possible length-to-depth ratios between 0.23~and~2.75. This length and depth range was determined based on previous experimental results that found resonant tones occurring for length-to-depth ratios $\leq 2.5~\text{at}$ airspeeds $\leq 60~\text{m/s}$.

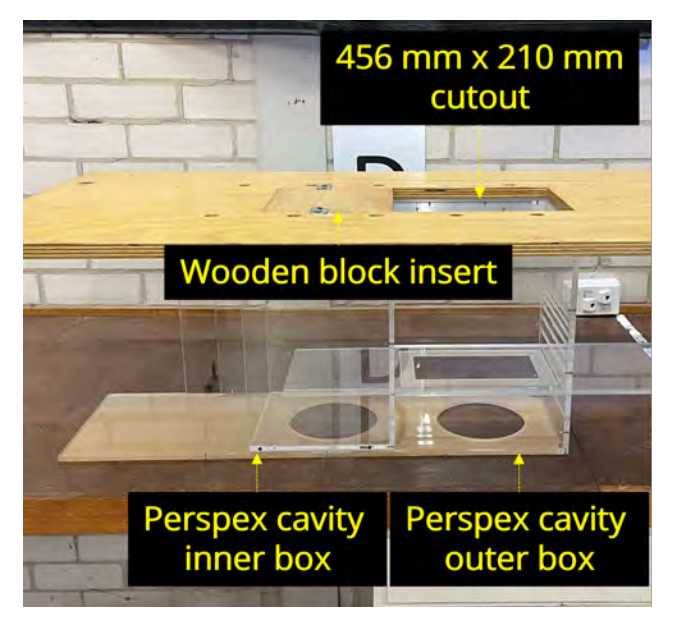


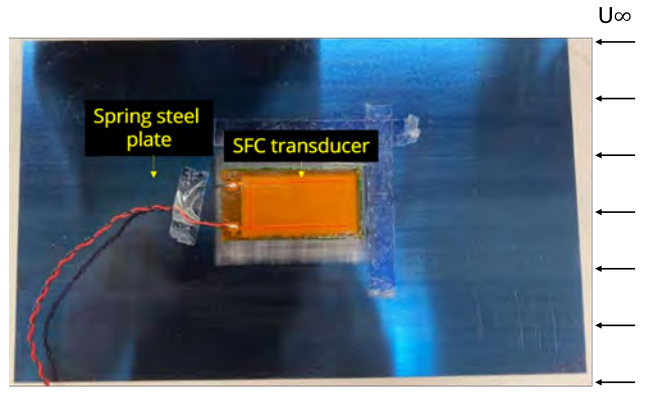


Figure 6 – Perspex cavity fitted to wind tunnel wooden floor test section.

Figure 7 – Perspex cavity fitted to wind tunnel test section.

2.2 Harvester devices

Each energy harvester device consists of a 0.175 mm thick [011] poled $Mn - Pb(Mg_{1/3}Nb_{2/3})O_3 - Pb(Zr,Ti)O_3(or\ Mn - PMN - PZT)$ SFC, bonded to 152 mm $\times 250$ mm $\times 0.381$ mm spring steel flat plate. The surface of the spring steel was prepared by marking it orthogonally with 600-grit wet and dry sandpaper. The surface was then cleaned with acetone and a thin layer of structural paste applied to the cleaned surface, before positioning the SFC in the desired location. This process ensured that the adhesive layer remained as thin as possible, without compromising the bonding phase.



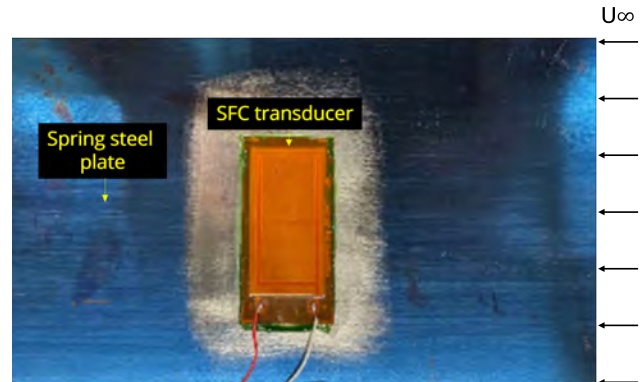


Figure 8 – Image of energy harvesting device - parallel.

Figure 9 – Image of energy harvesting device - perpendicular.

As shown in Figures 8 and 9, the SFC was bonded in parallel and perpendicular orientations with respect to the free stream airflow. The dimensions of the spring steel flat plate, specifically its length, width, and thickness, were chosen to ensure that the SFC transducer does not have authority over the stiffness of the plates.

Each harvester device was centrally mounted to the cavity floor panel using high-strength doublesided tape, with the transducer facing downward toward the laboratory floor for all lengths and depths tested, as highlighted in Figure 10.

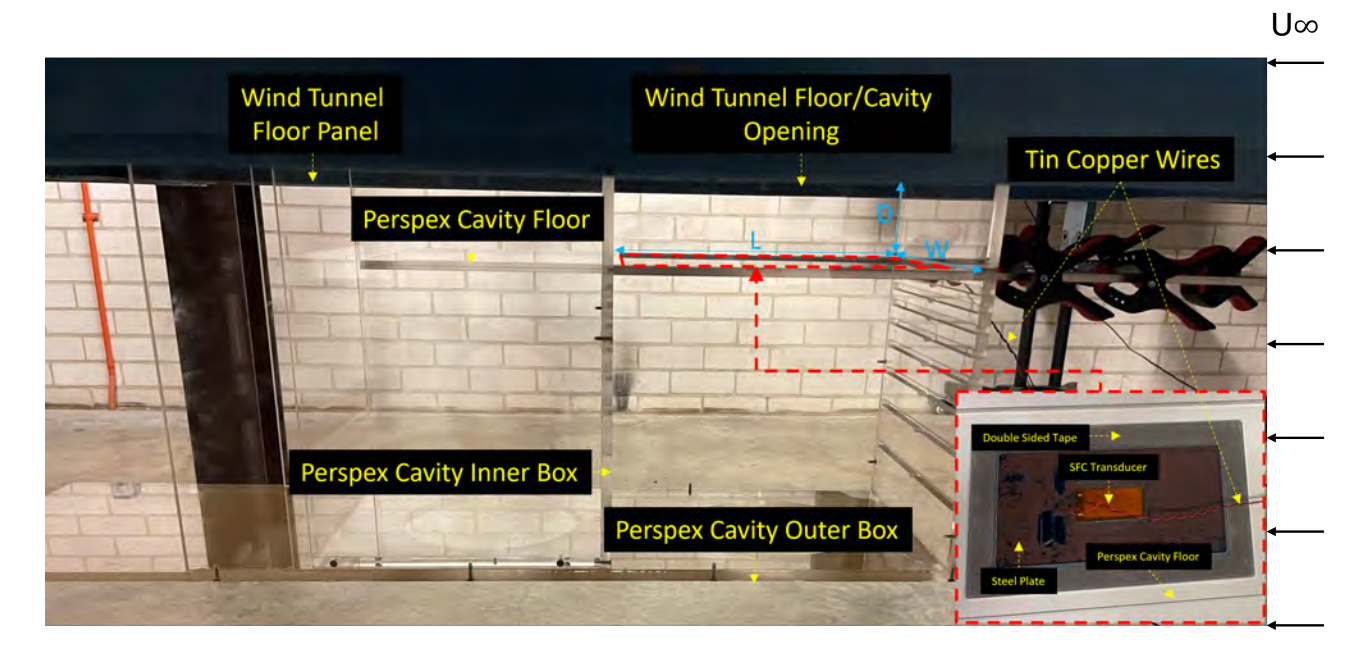


Figure 10 – Wind tunnel cavity experimental setup.

Thin copper wires were soldered to each terminal of the SFC, ensuring that the thermal conditions were kept as low as possible to prevent any phase transition and de-poling of the SFC.

2.3 Experimental Procedure

The experimental setup involved meticulous preparation to ensure accurate data collection and analysis. The copper wires leading from the SFC were connected to a resistance decade box, which was subsequently connected to an oscilloscope using an oscilloscope probe with an amplitude setting of $10\times$. This configuration allowed for precise measurements of the voltage output across different

resistances.

The range of resistances selected for this experiment, spanning from $1 \text{ k}\Omega$ to $30 \text{ k}\Omega$ at intervals of $2 \text{ k}\Omega$ and from $30 \text{ k}\Omega$ to $100 \text{ k}\Omega$ at intervals of $10 \text{ k}\Omega$, was based on previous work that analysed the impedance characteristics of the harvester device. This analysis indicated that resonant frequencies of the harvester occur within a resistance range between $1 \text{ k}\Omega$ to $30 \text{ k}\Omega$, making it essential to include these values to accurately capture the device's response to varying loads. Additionally, resistances up to $100 \text{ k}\Omega$ were tested to explore any interesting behavior or phenomena beyond the key range.

For each resistance value, 1 million samples were recorded over a 50-second interval, ensuring a low mean sample error and detailed voltage fluctuations. This extensive data collection was repeated for all lengths and depths at a wind tunnel airspeed of 60 m/s. This large dataset allowed analysis of the performance of the energy harvesting device, under varying loads.

To analyse the recorded voltage data and calculate the corresponding power, custom MATLAB code was developed. The code began with the extraction and organisation of data from the oscilloscope files. Once the data was extracted and organised, the power, peak power, and average power were calculated for all test cases.

The results were then visualised through various plots, generated by MATLAB. These plots included power curves, showing the relationship between resistance and power output for both peak power and average power.

3. Results and Analysis

The experimental analysis focused on identifying the cavity geometries that produced the maximum peak and average power outputs for the parallel and perpendicular configurations of the harvester devices.

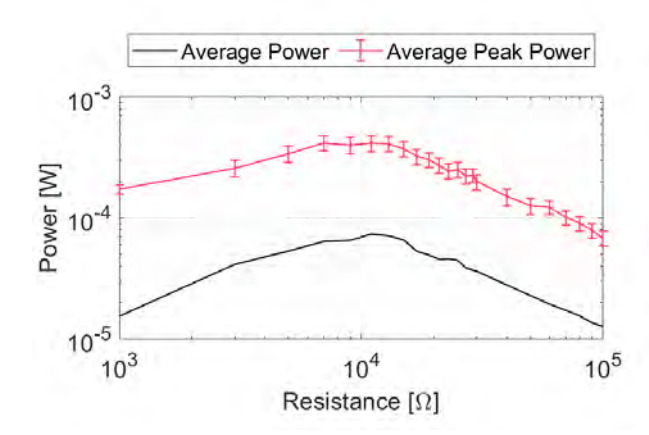
3.1 Peak and Average Power for parallel and perpendicular Devices

For the parallel harvester device, the maximum peak power was recorded at a cavity length of 190 mm and a depth of 325 mm, producing a peak power of 0.419 mW. As shown in Figure 11, the harvested power versus resistance plot for this configuration reveals a significant transient peak, indicating resonant interactions within the cavity structure. In particular, this configuration also yielded the highest average power for the parallel device, with an average power of 0.0738 mW, highlighting its effectiveness in this specific geometric setup.

In comparison, the perpendicular harvester device under the same geometric conditions of 190 mm length and 325 mm depth exhibited a significantly higher peak power of 0.934 mW, as illustrated in Figure 12. This value is more than two times the peak power achieved by the parallel device. The average power for the perpendicular device in this configuration was 0.0430 mW. Despite the average power being lower than the peak, the perpendicular device demonstrated a higher overall efficiency compared to the parallel device.

For the perpendicular harvester device, the maximum peak power was recorded at a cavity length of 418 mm and a depth of 151 mm, producing a peak power of 2.59 mW. As shown in Figure 14, the harvested power versus resistance plot for this configuration shows a substantial peak. The average power for this configuration was 0.106 mW.

In comparison, the parallel harvester device under the same geometric conditions of 418 mm length and 151 mm depth exhibited a peak power of 0.101 mW, as illustrated in Figure 13. The average power for the parallel device in this configuration was again significantly lower, at 0.00263 mW. These results further emphasise the performance of the perpendicular device.



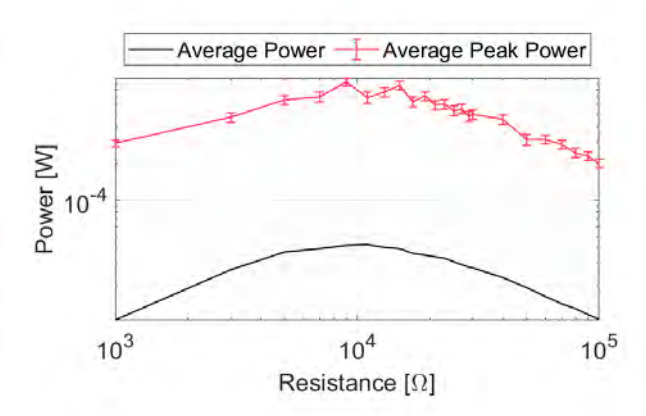
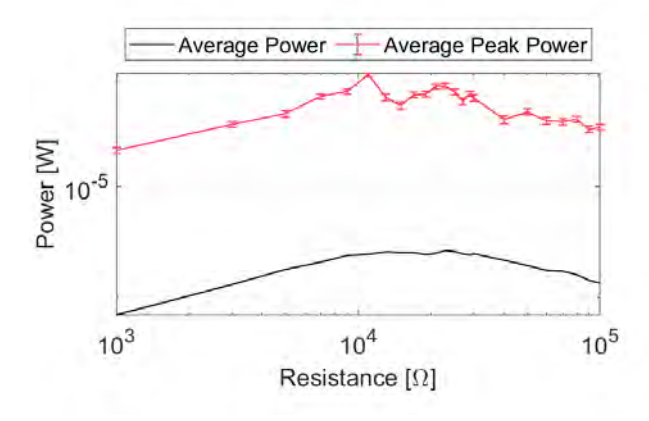


Figure 11 – Harvested power vs resistance for L = 190 mm, D = 325 mm and free stream velocity = 60 m/s - parallel harvester device.

Figure 12 – Harvested power vs resistance for L = 190 mm, D = 325 mm and free stream velocity = 60 m/s - perpendicular harvester device.



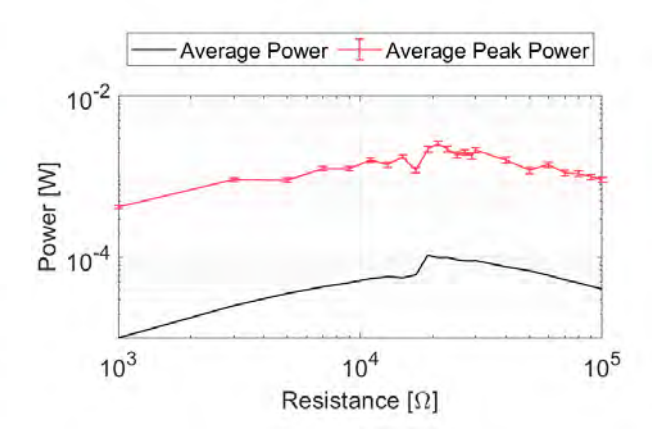
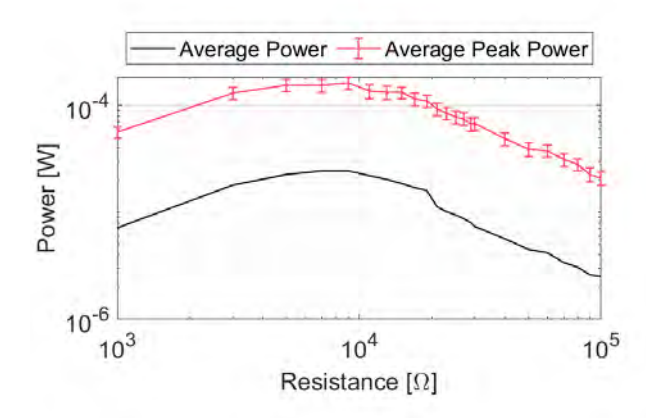


Figure 13 – Harvested power vs resistance for L = 418 mm, D = 151 mm and free stream velocity = 60 m/s - parallel harvester device

Figure 14 – Harvested power vs resistance for L = 418 mm, D = 151 mm and free stream velocity = 60 m/s - perpendicular harvester device

For the perpendicular harvester device, the maximum average power was recorded at a cavity length of 152 mm and a depth of 325 mm, producing an average power of 0.149 mW. As shown in Figure 16, the harvested power versus resistance plot for this configuration demonstrates a consistent and substantial power output. The peak power for this configuration was 1.47 mW.

In comparison, the parallel harvester device under the same geometric conditions of 152 mm length and 325 mm depth exhibited a significantly lower average power of 0.0244 mW, as illustrated in Figure 15. The peak power for the parallel device in this configuration was 0.163 mW. These results reinforce the observation that the perpendicular orientation consistently outperforms the parallel orientation in terms of peak power by approximately 100% and average power outputs by approximately 200% across all cavity geometries.



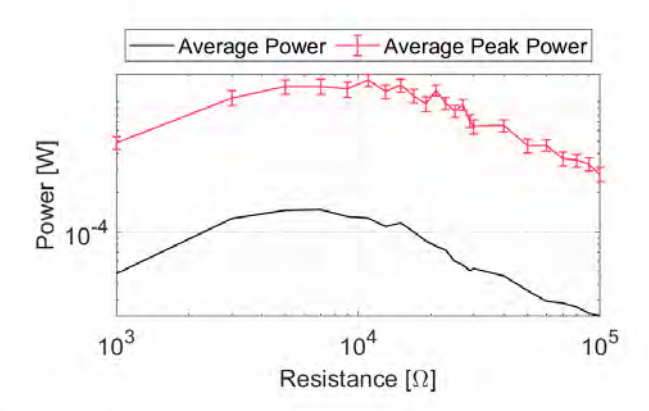


Figure 15 – Harvested power vs resistance for L = 152 mm, D = 325 mm and free stream velocity = 60 m/s - parallel harvester device

Figure 16 – Harvested power vs resistance for L = 152 mm, D = 325 mm and free stream velocity = 60 m/s - perpendicular harvester device

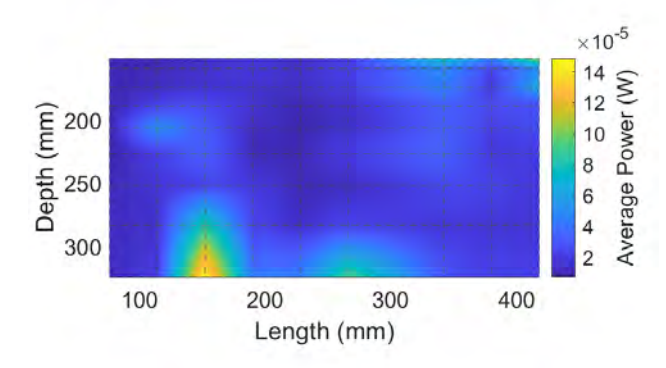
3.2 Maximum Peak and Maximum Average Power for Lengthwise and Crosswise Devices

Surface plots of the harvested maximum average power for all cavity geometries using the perpendicular harvester device reveal several key trends. Figure 17 shows the variation in average power output as a function of cavity length and depth. The plot clearly highlights the highest average power occurring at a length of 152 mm and a depth of 325 mm, producing an average power of 0.149 mW.

Notable secondary peaks can be observed around lengths of 284 mm and depths of 325 mm, indicating that certain length-to-depth ratios are particularly conducive to maximising power output. These secondary peaks, although lower than the primary maximum, still represent significant peaks in power and highlight the versatility of the perpendicular harvester device in various cavity setups.

A closer look at the trends shows that higher average power outputs are achieved at deeper cavity configurations, particularly at depths greater than 250 mm. The lowest power outputs are observed at shallower depths, particularly for cavity lengths below 200 mm, where the power output drops significantly. This suggests that deeper cavities provide a more favorable environment for the perpendicular harvester device to capture aeroacoustic energy.

Examining the corresponding resistance values in Figure 18 provides further insight into the optimal conditions for energy harvesting. There is a discernible relationship between the higher range of power outputs and a specific resistance range. The highest power outputs tend to occur within a resistance range of approximately $7~\mathrm{k}\Omega$ to $17~\mathrm{k}\Omega$.



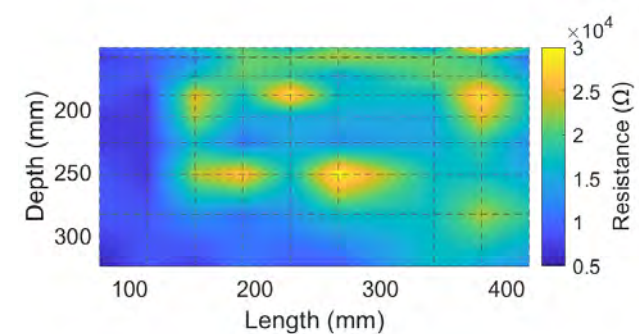


Figure 17 – Harvested maximum average power as a function of cavity length and depth at free stream velocity = 60 m/s - perpendicular harvester device.

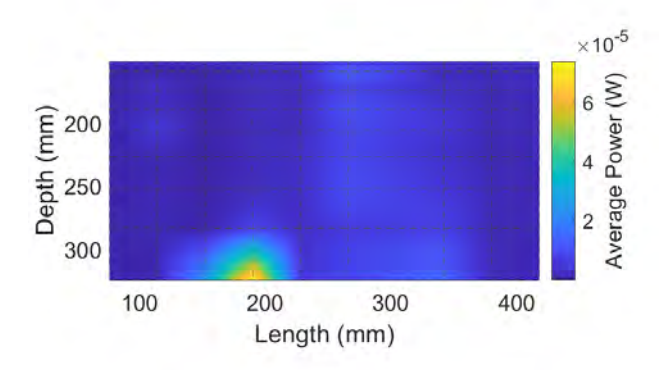
Figure 18 – Max average power corresponding resistance as a function of cavity length and depth at free stream velocity = 60 m/s - perpendicular harvester device.

The surface plots of the harvested maximum average power for all cavity geometries using the parallel harvester device reveal several distinct trends, some of which mirror those observed with the perpendicular harvester device. Figure 19 shows the variation in average power output as a function of cavity length and depth. The highest average power for the parallel device occurs at a length of 190 mm and a depth of 325 mm, producing an average power of 0.074 mW. This peak, although different in magnitude, suggests that similar geometric configurations can enhance the energy harvesting efficiency for both orientations.

Secondary peaks in power output are observed at lengths of 152 mm and depths of 325 mm, as well as lengths of 76 mm and depths of 325 mm. These secondary maxima, though lower than the primary peak, are consistent with the multiple optimal configurations identified for the perpendicular harvester device. This indicates that both devices exhibit a level of versatility in various cavity setups, though the specific geometries yielding peak performance differ slightly between the two.

A closer look at the results reveals that higher average power outputs for the parallel device, are achieved at deeper cavity configurations, particularly at depths greater than 250 mm. Conversely, the lowest power outputs are consistently observed at shallower depths and cavity lengths below 200 mm. This suggests that deeper cavity geometries provide a more favorable environment for capturing aeroacoustic energy, regardless of the harvester's orientation.

For the parallel harvester, the resistance value associated with the maximum average power at a cavity length of 190 mm and depth of 325 mm is 11 k Ω , where for the perpendicular device it was 7 k Ω at a cavity length of 152 mm and depth of 325 mm. The relationship between higher power outputs and specific resistance ranges is evident in both devices. For the parallel harvester, the highest power outputs occur within a resistance range of approximately 7 k Ω to 11 k Ω , similar to the perpendicular device which was 7 k Ω to 17 k Ω . This consistency highlights the critical role of tuning the resistance to enhance the energy harvesting performance across different geometric configurations.



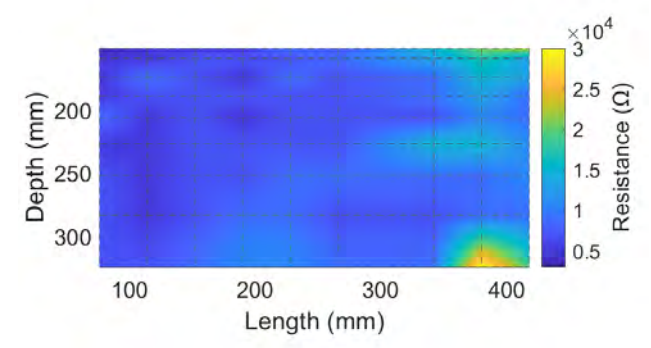


Figure 19 – Harvested maximum average power as a function of cavity length and depth at free stream velocity = 60 m/s - parallel harvester device.

Figure 20 – Max average power corresponding resistance as a function of cavity length and depth at free stream velocity = 60 m/s - parallel harvester device.

4. Conclusions

This work has demonstrated that a piezoelectric SFC transducer can effectively harvest electrical energy from aeroacoustic excitation in a rectangular cavity. Varying the orientation of the piezoelectric material from parallel to perpendicular, with respect to the free stream airflow, resulted in a minimum two times increase in the amount of energy harvested for equivalent cavity geometries.

For all geometries tested, the perpendicular device outperformed the parallel device by approximately 100% in terms of peak power output and around 200% when analysing the average power output. Specifically, the maximum peak power recorded was 2.59 mW at a cavity length of 418 mm and a depth of 151 mm for the perpendicular device, compared to 0.419 mW for the parallel device at a cavity length of 190 mm and a depth of 325 mm. Similarly, the maximum average power for the perpendicular device was 0.149 mW at a cavity length of 152 mm and a depth of 325 mm, while the parallel device achieved 0.074 mW under the same conditions.

Further evaluation of the experimental data focused on analysing trends related to the power output of the harvester devices and its correlation with various cavity geometries for both devices. A closer inspection of the secondary peaks in power output at specific lengths and depths suggests that both devices exhibit a level of versatility in various cavity setups, although the specific geometries yielding peak performance differ slightly. Secondary peaks in power output were observed at lengths of 152 mm and depths of 325 mm, as well as lengths of 76 mm and depths of 325 mm. These secondary peaks, although lower than the primary peak, are consistent with the multiple optimal configurations identified for the perpendicular harvester device. This indicates that both devices exhibit versatility in various cavity configurations.

These results underscore the potential of using piezoelectric SFC transducers for energy harvesting in high-energy cavity environments, with the perpendicular orientation proving to be significantly more effective. This insight is crucial for the design and implementation of energy harvesting systems in aerospace applications, providing a sustainable power source for Structural Health Monitoring systems.

5. Contact Author Email Address

James Matthew Kirkness, email: james.kirkness@sydney.edu.au

6. Acknowledgments

The Advanced Piezoelectric Materials and Applications Program is supported by DMTC Limited (Australia) and funded by Defense Science and Technology Group through the Next Generation Technologies Fund.

7. Copyright Statement

The authors confirm that they, and/or their company or organisation hold copyright on all of the original material included in this paper. The authors also confirm that they have obtained permission, from the copyright holder of any third party material included in this paper, to publish it as part of their paper. The authors confirm that they give permission, or have obtained permission from the copyright holder of this paper, for the publication and distribution of this paper as part of the ICAS proceedings or as individual off-prints from the proceedings.

References

- [1] Grover H.J. *Fatigue of aircraft structures*. 1st edition, US Government Printing Office Washington, DC, 1966.
- [2] Jones M.B, Watmuff J. Aero-acoustic measurements of a deep cavity in low-speed flow. *17th Australasian Fluid Mechanics Conference*, Auckland, New Zealand, 2007.
- [3] Rossiter J.E. Wind-tunnel experiments on the flow over rectangular cavities at subsonic and transonic speeds. 1st edition, Ministry of Aviation, 1964.
- [4] Dowell E.H., Hall K.C. Modeling of fluid-structure interaction. *Annual Review of Fluid Mechanics*, Vol. 33, pp. 445-490, 2001.
- [5] Giurgiutiu V. *Structural Health Monitoring with Piezoelectric Wafer Active Sensors*. 2nd edition, Academic Press, 2014.
- [6] Schipper M, Munk D, Gray J, Moss S, Rajic N, Smith C, Kirkness J, Vio G, Szydzik C, Mitchell A. Aeroacoustic energy harvesting using relaxor ferroelectric single crystals. Proc 9th Asia-Pacific Workshop on Structural Health Monitoring, Cairns, Vol. 27, pp. 95-102, 2023.
- [7] Farrar C.R., Worden K. Structural Health Monitoring: A Machine Learning Perspective. John Wiley & Sons, 2012.
- [8] Giurgiutiu V. Structural Health Monitoring with Piezoelectric Wafer Active Sensors. Academic Press, 2014.
- [9] Staszewski W.J., Boller C., Tomlinson G.R. *Health Monitoring of Aerospace Structures: Smart Sensor Technologies and Signal Processing.* John Wiley & Sons, 2004.
- [10] Yin S., Liu J., Cong B. Review of thermal runaway monitoring, warning, and protection technologies for lithium-ion batteries. *Processes*, Vol. 11, No. 8, pp. 2345, 2023.
- [11] Smith C. An experimental investigation of flow induced pressure oscillations in rectangular cavities. *AIAA Scitech 2021 Forum*, Surfers Paradise, Vol. 1, pp. 2-16, 2019.
- [12] Brusa E., Carrera A., Delprete C. A review of piezoelectric energy harvesting: Materials, design, and readout circuits. *Actuators*, Vol. 12, No. 12, pp. 457, 2023.
- [13] Ghazanfarian J., Mohammadi M.M., Uchino K. Piezoelectric energy harvesting: A systematic review of reviews. *Actuators*, Vol. 10, No. 12, pp. 312, 2021.